



# Experimental investigation on the effect of pulsating flow on heat transfer and pressure drop in conical tubes

Mohamed T. Abdelghany<sup>1</sup> · Samir M. Elshamy<sup>1</sup> · M. A. Sharafeldin<sup>2</sup> · O. E. Abdellatif<sup>2</sup>

Received: 29 January 2023 / Accepted: 3 April 2023 / Published online: 12 May 2023  
© The Author(s) 2023

## Abstract

In order to boost the heat transfer rate in a conical coiled tube (CCT) using an active technique, a solenoid valve was placed ahead of the CCT and employed as a pulse generator in this research. Experimentally, the effect of pulsation on heat transfer and pressure drop in the CCT was investigated. Experiments were conducted for pulsating flow throughout a Womersley number ( $Wo$ ) range of 30–48, which corresponds to a pulsating frequency of 4–10 Hz, a Dean number ( $De$ ) of 1148–2983, and a coil torsion ( $\lambda$ ) of 0.02–0.052. Results revealed that pulsating flow yields larger  $Nu$  values than steady flow. A rise in heat transfer characteristics is achieved by decreasing both the pulse frequency and the coil torsion. A pulsating flow at 4 Hz ( $Wo = 30$ ) was shown to promote heat transfer by the most of all the examined frequencies. The average  $Nu$  increases as  $De$  increases, although the friction factor often decreases as  $De$  increases. When the coil torsion is reduced from 0.052 to 0.02 while maintaining the same  $De$  and  $Wo$ , the average  $Nu$  and  $f$  increase by 23% and 30%, respectively. A correlation for the average Nusselt number and friction factor was presented, taking frequency and coil torsion into account.

**Keywords** Conical tubes · Pulsating flow · Coil torsion · Heat transfer · Friction factor

## List of symbols

$A$	Area ( $m^2$ )
$C_p$	Specific heat ( $J\ kg^{-1}\ C^{-1}$ )
$d$	Diameter ( $m$ )
$F$	Frequency (Hz)
$h$	Convection heat transfer coefficient ( $W\ m^{-2}\ C^{-1}$ )
$I$	Current (A)
$K$	Thermal conductivity ( $W\ m^{-1}\ C^{-1}$ )
$L$	Length (m)
$\dot{m}$	Mass flow rate ( $Kg\ s^{-1}$ )
$P_c$	Pitch (m)
$P$	Perimeter of tube (m)
$Q^\circ$	Rate of heat transfer (W)
$q^\circ$	Heat flux ( $W\ m^{-2}$ )
$S$	Spacing of coiled tube (m)
$T$	Temperature ( $^\circ C$ or $^\circ K$ )
$U$	Velocity ( $m\ s^{-1}$ )
$V$	Voltage (v)
$x$	Distance (m)

## Subscripts

avg	Average
c	Coil
cr	Critical
i	Inlet
o	Outlet
L	Large
s	Steady, small
t	Tube
w	Wall
x	Local variable

## Greek letters

$\delta$	Coil curvature ratio ( $d_{t,i}/D_c$ )
$\lambda$	Coil torsion ( $P_c/\pi D_c$ )
$\Pi Pi$	$\equiv$ A mathematical constant $\cong 3.1416$
$\rho$	Density ( $kg\ m^{-3}$ )
$f$	Friction factor
$\Gamma$	Period of the pulsation
$\theta$	Cone angle
$\phi$	Nanofluids concentration
$\mu$	Dynamic viscosity

## Dimensionless groups

$De$	Dean number
$Nu$	Nusselt number
$Pr$	Prandtl number

✉ M. A. Sharafeldin  
mahmoud.hassan@feng.bu.edu.eg

<sup>1</sup> High Institute of Engineering, October 6 City, Egypt

<sup>2</sup> Mechanical Engineering Department, Faculty of Engineering at Shoubra, Benha University, Banha, Egypt

Re Reynolds number  
 Wo Womersley number

### Abbreviations

CCT Conically coiled tube  
 CuO Copper oxide  
 HCT Helically coiled tube  
 He Helical number  
 PEC Performance evaluation criteria  
 SCT Spirally coiled tube  
 SiO<sub>2</sub> Silicon dioxide  
 TiO<sub>2</sub> Titanium dioxide

## Introduction

The idea of improving heat transfer within tubes, one of the most significant engineering applications where heat transfer coefficients are minimal, has received considerable attention. Pulsating is one of several techniques used to produce separation in the flow and increase the coefficient of heat transfer in internal flows. Creating time-varying flow, or pulsating flow, is thought to be an active method for enhancing convective heat transfer. In this work, two distinct techniques for enhancing heat transfer (pulsating flow and conically coiled tubes) are combined to improve heat transfer.

Widespread uses for coiled tubes include heating systems, chilled water systems, ground water systems, and residential usage. These applications are prevalent in several industries, including the chemical, biological, petrochemical, mechanical, and medicinal sectors. This extensive use of coiled tubes is a result of their compactness and shape, which promotes effective fluid mixing and increases heat transfer coefficients. Due to the considerable usage of coiled tubes in these applications, it is crucial to understand their heat transfer and pressure drop characteristics. Sheeba et al. [1] investigated experimentally and numerically the heat transfer characteristics and flow parameters of fully developed flow in a conical coiled tube heat exchanger in counter flow mode. Dean number and cone angle have a significant impact on heat transfer. The research drew the following conclusions: (i) the inner Nu is impacted by the inner and outer Dean numbers, and (ii) the ratios of mass flow rates of hot and cold fluids have a substantial effect on heat transfer and hence the efficacy of the heat exchanger. Purandare et al. [2] investigated pressure drop and the heat transfer properties of the CCT heat exchanger with varying cone angles, tube diameters, and mass flow rates. The findings demonstrated that the Nu rises as the Re within the tube increases. In addition, the findings demonstrated that when cone angle rises,  $f$  increases for a given Re.

Heyhat et al. [3] examined the effect of nanofluids and CCT geometric parameters on pressure drop and heat

transfer. Experiments were conducted with various concentrations of SiO<sub>2</sub>/water under laminar conditions. As geometric variables, several cone angles and coil pitches were used. According to the results, increasing the coil pitch enhances the heat transfer rate. Moreover, cone angle variation enhances heat transfer more effectively than coil pitch change. Abdelmagied [4] performed experimental and numerical analysis of the thermal performance of a triple CCT heat exchanger. In all studies, the triple CCT heat exchanger performed better in terms of Nu than the double CCT heat exchanger by 127.5% when they were both set up to work in a counter-flow configuration. Results also showed that raising the temperature of the water coming in makes the system more efficient while lowering the Nu. Abdelghany et al. [5, 6] studied experimentally two tube geometries, CCT and HCT, utilizing a variety of coil torsions while preserving the same curvature ratio. According to the findings, the Nu and  $h$  rise when the coil's torsion decreases. Al-Salem et al. [7] investigated steady-state heat transfer and fluid flow in the annulus portion of a tube-in-tube conically coiled heat exchanger. The findings permitted the development of two correlations for estimating the annulus section exergy efficiency and exergy performance coefficient. Furthermore, the thermal and hydraulic properties of coiled tubes have been the subject of several investigations [8–16]. Some correlations were reported in these research' outcomes for forecasting the Nusselt number, friction factor, total heat transfer coefficient, and so on.

Khosravi-Bizhaem et al. [17] conducted an experiment to study the effects of pulsating flow on heat transfer and friction factor in HCT. Experiments were conducted for a range of Re between 2000 and 9500 and Womersley numbers between 16 and 40. They evaluated the Nusselt number and fanning friction factor in constant flow with the known correlations in the literature and found an exceptional degree of agreement. Zohir et al. [18] examined the effects of pulsation with varied amplitudes on rates of heat transfer in a double-pipe heat exchanger with a coiled wire positioned on the outside surface of the inner tube. Experiments are conducted for Re values between 4000 and 12,000. The experimental findings revealed that heat transfer rates rise as the pitch of coiled wire increases.

Pan et al. [19, 20] have determined the mechanism by which sinusoidal pulsing flow enhances heat transfer in HCT. Compared to continuous flow, the volume average field synergy angle was 2.45% lower for pulsed flow. Zhang et al. [21] observed that square wave pulsing flow produced greater fluid disturbance and promoted fluid mixing more easily. Therefore, it may be desirable to boost heat transfer. Using computational techniques, Yu et al. [22] studied the flow and heat transfer properties of pulsating laminar flow within a heated square cylinder. The results were analyzed at a Reynolds number of 100, which was kept constant. The

amplitude of the pulsation varied between 0.2 and 0.8, while the frequency ranged from 0 to 20 Hz. The findings revealed that the heat transfer enhancement increased with the increment of the flow pulsation amplitude. The heat transfer enhancement factor peaks when the pulsing frequency is inside the lock-on regime. This is caused by the narrowing of the vortex forming region.

Li et al. [23, 24] examined numerically the effect of square-wave pulsing flow in a HCT on heat transfer enhancement. The numerical results agree with the experimental outcomes. Results indicate that both the Nusselt number and the flow resistance coefficient increase as amplitude and Womersley number values rise. Guo et al. [25] conducted a numerical analysis of nanofluid heat transfer performance in a helical coil under pulsation, detailing the impact of frequency of pulsation and Re on heat transfer performance. Regarding the purview of Re, the findings demonstrated an optimal pulsation frequency for enhancing heat transfer. Under pulsation, the secondary flow created in the cross area and the counter-rotating vortex produced axially contribute to the enhancement of the helical coil's heat transfer. Moreover, the subject of pulsating flow has been the focus of a lot of previous research [26–30]. The recent literature on heat transfer and pressure drop in coiled tubes is summarized in Table 1.

The literature reviews show that there hasn't been enough research done on the flow field and heat transfer characteristics of the square wave pulsating flow in the conical coiled tubes (CCTs) [23]. Consequently, the objective of this work is to investigate the effects of pulsating flow phenomena on pressure drop and heat transfer characteristics in CCTs. Pulsation frequency, Womersley number, coil torsion, Dean number, and tube side flow rate are all aspects of better heat transfer that have been investigated for their potential implications.

## Experimental setup and procedures

Figure 1 depicts a photograph of the experimental setup and its schematic diagram. As the testing fluid in a closed loop, water maintained at a temperature of 25 °C was employed. The main cycle includes a water tank, a centrifugal pump, a solenoid valve, an accumulator, a cooling system, and CCT. The following is the technique for setting up. The water was pumped from the tank using a centrifugal pump, cycled through the CCT, and then returned to the tank. The solenoid valve was connected to the Arduino Uno board through a relay module to create the square wave pulsation. The solenoid valve can open and close automatically at a regular time interval, and this is done through code written on the Arduino IDE program, and the same square-wave pulsating

mechanism was used in recent work by Khosravi-Bizhaem et al. [17] and Li et al. [23, 24]. In a square wave with a 4 Hz pulsation frequency, the solenoid valve opens and closes four times per second. Therefore, a square wave with an opening and closing period of 0.125 s was formed. An accumulator was placed in front of the solenoid valve so that pressure variations brought on by flow pulsations would no longer occur, as well as to protect the pump from being damaged. An electrical heater that was well insulated and looped around a CCT was used to provide a heat flux that was uniform throughout. In order to remove heat from the water in the cooling tank, a cooling system with a horsepower rating of 0.5 is used. In order to keep the temperature of the cold water input constant, a system that is regulated by a thermostat is used.

During the experiment, three test sections consisting of 45° angle conical coiled tubes were used. In Table 2, geometrical characteristics of CCTs are outlined. Copper M-type tubes were used in the process of manufacturing the CCTs. K-type thermocouples were installed at various intervals along the CCTs in order to determine the temperature of the wall surface in parts that were thermally developing and regions that were thermally completely formed. Thermocouples were connected to data acquisition equipment, and LabVIEW software was used to transport temperature data from the equipment to a laptop. In order to achieve steady-state conditions, an experiment must be run for nearly half an hour at the beginning, followed by another 10 min during which the flow rate is varied. After the system has reached a steady state, all of the parameters will have been measured and written down. After that, the flow rate was altered to achieve the new needed value, and the procedure that came before it was carried out once again.

This study has some important definitions of some parameters that have an important impact. The coil curvature ( $\delta$ ) is defined as the ratio of the inner diameter of the CCT ( $d_{t,i}$ ) to the mean diameter of the coil curvature ( $D_c$ ), and the coil torsion ( $\lambda$ ) is the ratio of the coil pitch to the length of one completed turn.

$$\delta = \frac{d_{t,i}}{D_c} \quad (1)$$

$$\lambda = \frac{P_c}{\pi D_c} \quad (2)$$

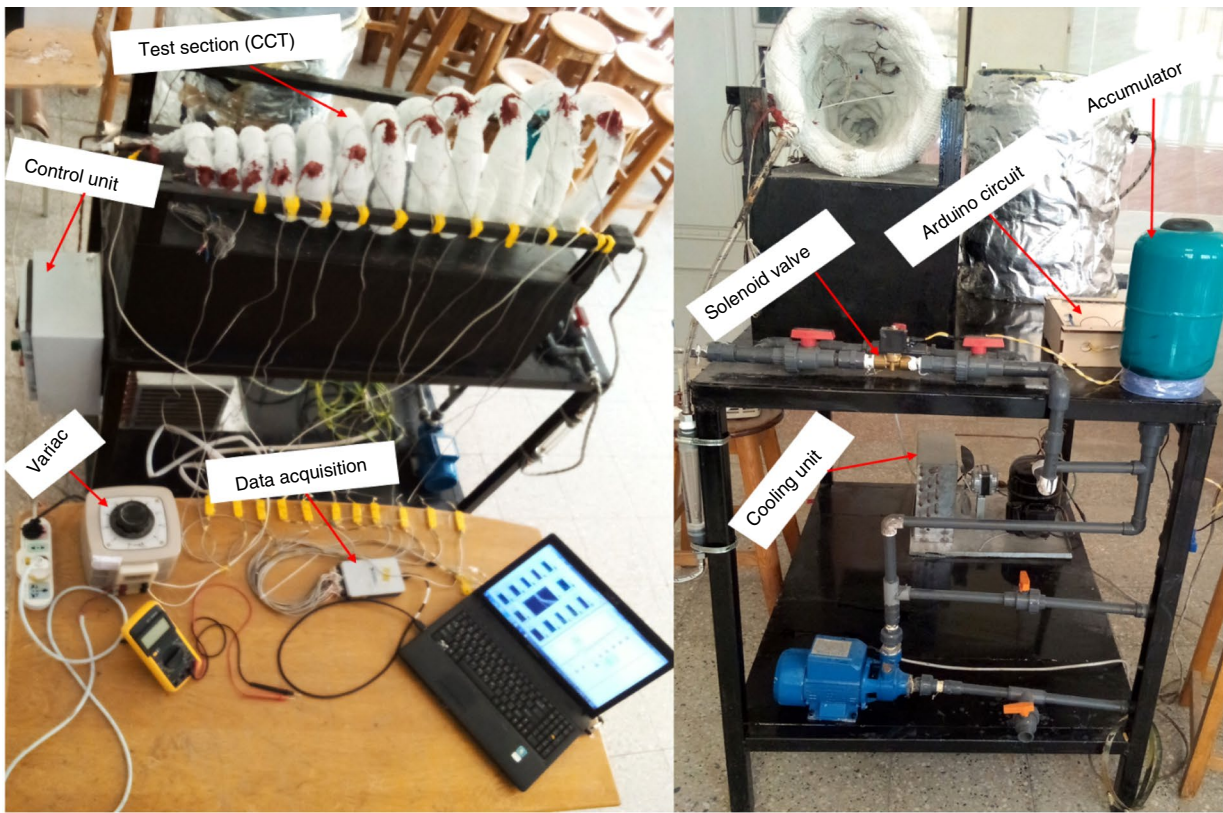
Non-dimensional parameter Dean number (De) is used to describe the fluid flow in a CCT and is represented as

$$De = Re\sqrt{\delta} \quad (3)$$

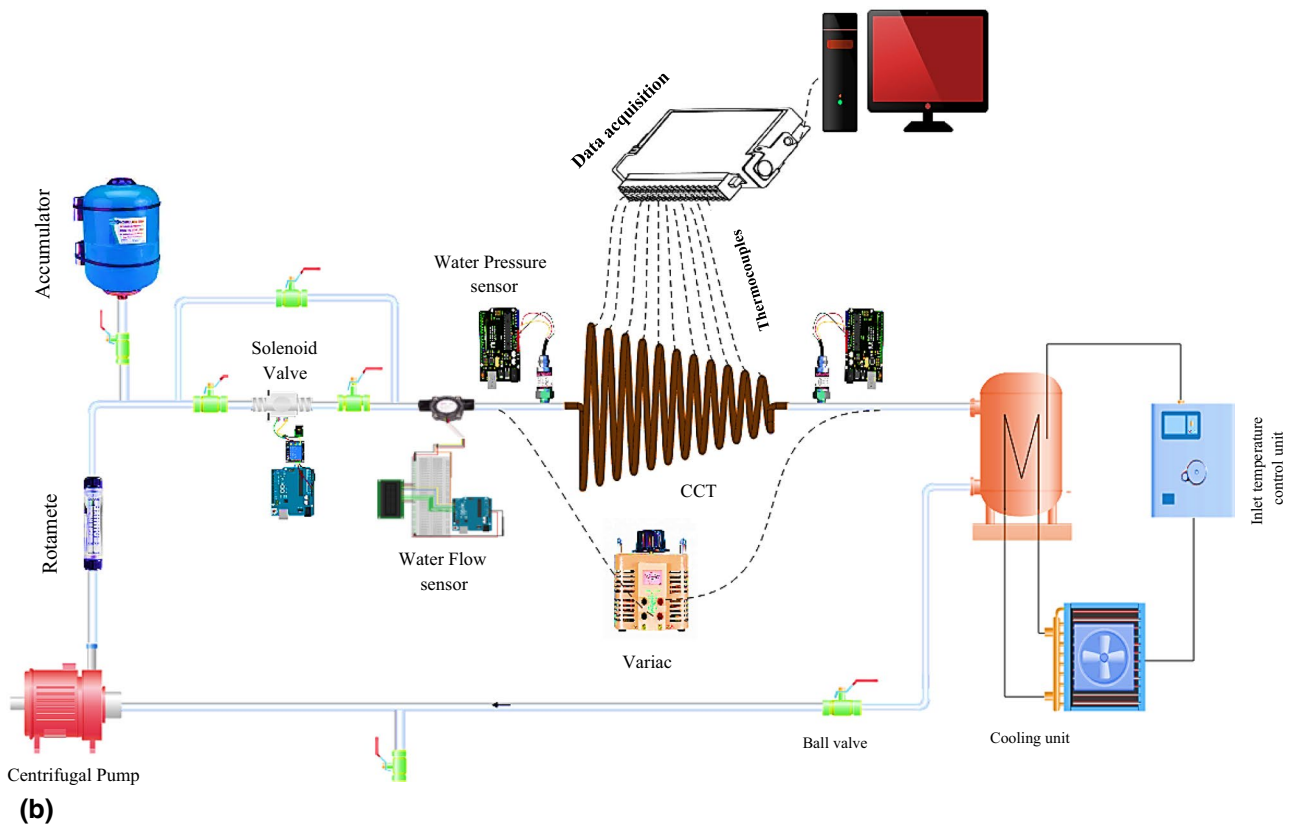
Womersley number (Wo) is used to describe the pulsating flow and is defined as follows:

**Table 1** An overview of recent research on heat transfer and pressure drop in coiled tubes

References	Year	Approach	Geometry	Flow type	Working fluid	Applicable conditions
Naphon and Wiriyasart [26]	2017	Experimental	SCT	Pulsating flow	TiO <sub>2</sub> /water nanofluids	$P_C = 20.5$ mm $0.04 \leq \delta \leq 0.06$ $0.02 \leq \dot{m} \leq 0.05$ kg s <sup>-1</sup> $10 \leq F \leq 20$ Hz $0.25 \leq \phi \leq 0.5\%$
Pan et al. [20]	2018	Numerical	HCT	Oscillating flow	Helium-4	$P_C = 30$ mm $D_C = 75$ mm $L_t = 222$ mm $1 \leq F \leq 30$ Hz $5 \leq U \leq 12$ m s <sup>-1</sup>
Wang et al. [8]	2019	Experimental and numerical	HCT	Steady	Water	$D_C = 92$ mm $2000 \leq Re \leq 10,000$ $6.99 \leq Pr \leq 104.99$
Khosravi-Bizhaem et al. [17]	2019	Experimental	HCT	Pulsating Flow	Water	$350 \leq He \leq 2300$ $2000 \leq Re \leq 9500$ $3 \leq Pr \leq 5.5$ $16 \leq Wo \leq 38$
Sheeba et al. [1]	2020	Experimental and numerical	CCT	Steady	Water	$\lambda = 0.0397$ $\theta = 72$ $0.2 \leq \dot{m} \leq 0.7$ lpm $90 \leq De \leq 1000$ $3 \leq Pr \leq 4$
Heyhat et al. [3]	2020	Experimental	CCT	Steady	SiO <sub>2</sub> / water nanofluids	$1050 \leq Re \leq 2150$ $0^\circ \leq \theta \leq 60^\circ$ $0 \leq \phi \leq 0.3\%$
Abdelmagied [9]	2020	Experimental and numerical	CCT	Steady	Water	$0.035 \leq \lambda \leq 0.111$ $0^\circ \leq \theta \leq 90^\circ$ $485 \leq De \leq 6200$ $2.8 \leq Pr \leq 4.75$ $0.016 \leq \dot{m} \leq 0.3$ kg s <sup>-1</sup>
Shiravi et al. [31]	2021	Experimental	HCT	Steady	Carbon black nanofluid	$10,000 \leq Re \leq 31,500$ $0 \leq \phi \leq 0.4\%$ $1 \leq \dot{m} \leq 7$ l/min
Li et al. [23]	2023	Numerical	HCT	Pulsating Flow	Water	$\lambda = 0.08$ $\delta = 0.0344$ $1400 \leq Re \leq 8950$ $0.03 \leq \dot{m} \leq 0.3$ m <sup>3</sup> /hr $3 \leq Wo \leq 27$
Tuncer et al. [32]	2023	Experimental	HCT	Steady	TiO <sub>2</sub> /water and CuO–TiO <sub>2</sub> /water nanofluids	$D_C = 100$ mm $P_C = 16$ mm $6600 \leq Re \leq 16,000$ $\phi = 1\%$
Sundar and Shaik [33]	2023	Experimental	HCT	Steady	Water+ ethylene glycol mixture based nanodiamond nanofluids	$D_C = 116$ mm $P_C = 25$ mm $249 \leq De \leq 1144$ $15.27 \leq Pr \leq 37.12$ $0.2 \leq \phi \leq 1\%$
Present study	2023	Experimental	CCT	Pulsating flow	Water	$0.02 \leq \lambda \leq 0.052$ $\delta = 0.0564$ $30 \leq Wo \leq 48$ $4 \leq F \leq 10$ Hz $\theta = 45$ $0.03 \leq \dot{m} \leq 0.09$ kg s <sup>-1</sup> $1148 \leq De \leq 2983$



(a)



(b)

Fig. 1 Experimental setup, a photograph view, and b schematic diagram

$$Wo = \frac{d_t}{2} \sqrt{\frac{2\pi F \rho}{\mu}} \quad (4)$$

where  $F$  is the pulsating frequency and  $\mu$  is the fluid's dynamic viscosity. In the current investigation, the value of  $F$  varies from 4 to 10 Hz.

Figure 2 depicts the stages involved in the fabrication of CCTs in which a uniform heat flux was supplied using an electrical heater wrapped around a CCT and well insulated by glass fiber and ceramic fiber. Twelve thermocouples of the K type were used to measure and record the temperatures after being checked for accuracy. The flow rate was measured using a water flow sensor (YF-S201) connected to an Arduino board and placed after the solenoid valve to know the flow pattern after the pulsation process. Two pressure sensors were connected to an Arduino board, and the LabVIEW Interface for Arduino (LIFA) was used to connect the Arduino board to the

LabVIEW software. We have built a code that can read both sensors simultaneously and measure the pressure drop without the need to read each sensor separately. Table 3 describes the apparatus used in the experimental setup.

## Methodology for data analysis

The following is how the Nu and friction factor were calculated in order to measure the rate of heat transfer and the drop in pressure that occurred in the CCTs. As a first step, the overall heat transfer rate and the heat flux in the CCTs were determined as follows:

$$Q^\circ = \dot{m}C_p(T_o - T_i), \quad \text{and} \quad Q^\circ = VI \quad (5)$$

$$\dot{q} = \frac{Q^\circ}{\text{Area}} \quad (6)$$

**Table 2** CCTs' geometrical characteristics

Coil no.	$\theta$	$D_c$ /mm	$S$ /mm	$P_c$ /mm	$L_c$ /mm	$d_{i,i}$ /mm	$\delta$	$\lambda$
#1	45°	200	0	12.7	165.1	11.28	0.0564	0.02
#2	45°		10	22.7	239.7			0.036
#3	45°		20	32.7	372.4			0.052

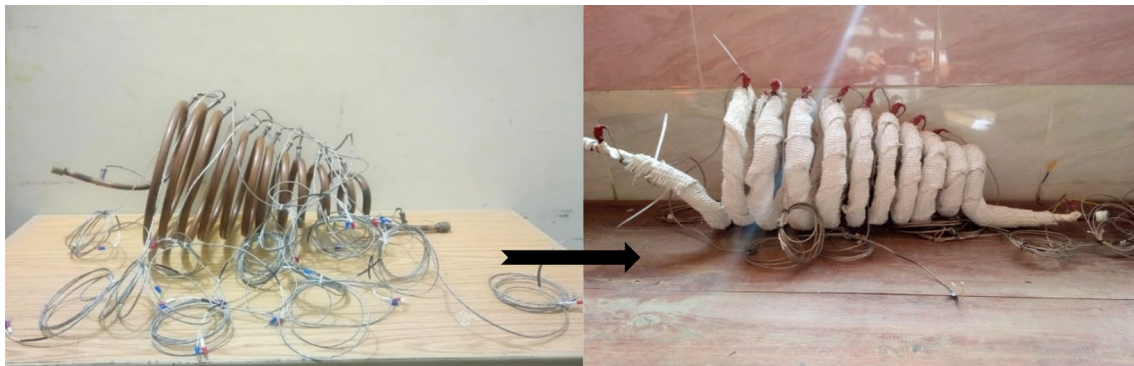


**Fig. 2** CCTs during fabrication process

**Table 3** Detailed descriptions of measurement equipment

Device	Description
Thermocouple	K-type The measuring range for temperature: 0–1023 °C Accuracy: $\pm 1.5$ °C Resolution: 0.25 °C
Water pressure sensor (SKU: SEN0257)	Pressure measurement range: 0 ~ 1.6 Mpa Measurement accuracy: 0.5 ~ 1%FS (0.5%, 0 ~ 55 °C) Operating temperature: – 20 ~ 85 °C
Water flow sensor (YF-S201)	Accuracy: between 2–60 L min <sup>-1</sup> $\pm 3\%$ Flow rate range: 0.5 ~ 60 L min <sup>-1</sup> Operating temperature: 0 ~ 80 °C

The outlet and inlet of the tube are denoted by the subscripts 'o' and 'i', respectively, while  $Q^\circ$  symbolizes the heat transfer rate,  $q^\circ$  represents the heat flux,  $m^\circ$  denotes the mass flow rate,  $C_p$  is the specific heat capacity, and  $T$  represents the temperature. The thermo-physical properties of water were measured at its mean temperature to establish a friction factor and heat transfer coefficient.

$$T_m = \frac{T_i + T_o}{2} \tag{7}$$

Here's how the local heat transfer coefficient and the local Nusselt number were found [34].

$$h_x = \frac{\dot{q}}{T_{w,x} - T_{m,x}} \tag{8}$$

$$Nu_x = \frac{h_x d}{K} \tag{9}$$

$T_{w,x}$  is the local wall temperature, which was recorded at the tube's outer wall surface using thermocouples installed on the coil wall, and  $T_{m,x}$  is the local mean fluid temperature, which was calculated using the given formula:

$$T_{m,x} = T_i + \frac{\dot{q}P}{\dot{m}C_p}x \tag{10}$$

where  $P$  is the tube's perimeter. The average heat transfer coefficient was computed numerically (using the trapezoidal rule) by integrating the local values across the tube's length as shown [35, 36]:

$$h_{avg} = \frac{1}{L} \int_0^L h_{(x)} dx \tag{11}$$

where  $L$  is the test segment. The average Nusselt number was calculated as follows [36].

$$Nu_{avg} = \frac{\dot{q}d_i}{K\Delta T_{avg}}, \Delta T_{avg} = \left[ \frac{1}{L} \int_0^L \frac{dx}{T_{w,x} - T_{m,x}} \right]^{-1} \tag{12}$$

The fanning friction factor was calculated as follows [34, 37]:

$$f = \frac{\Delta P_c d_{t,i}}{2L_t \rho_t U_t^2} = \frac{\Delta P_c \pi^2 \rho_t d_{t,i}^5}{32L_t \dot{m}_t^2} \tag{13}$$

### Uncertainty analysis

Holman [38] describes Kline and McClintock's more accurate approach for measuring experimental uncertainty. The approach is based on a detailed definition of the

uncertainties associated with the basic experimental data. Assume that  $R$  is a given function of the independent variables  $x_1, x_2, x_3, \dots, x_n$ . Thus  $R = R(x_1, x_2, x_3, \dots, x_n)$ . Let  $u_R$  represent the result's uncertainty and  $u_1, u_2, u_3, \dots, u_n$  represent the uncertainties in the independent variables. The result's uncertainty is expressed as:

$$u_R = \sqrt{\left(\frac{\partial R}{\partial x_1} u_1\right)^2 + \left(\frac{\partial R}{\partial x_2} u_2\right)^2 + \dots + \left(\frac{\partial R}{\partial x_n} u_n\right)^2} \tag{14}$$

The maximum uncertainties of  $De$ ,  $Nu$  and  $f$  for all experimental runs are around 1.4%, 4.3%, and 3.5%, respectively.

### Results and discussions

Studies were performed on three distinct CCTS, each of which had a different coil torsion ( $0.0202 \leq \lambda \leq 0.052$ ) but the same curvature ratio ( $\delta = 0.0564$ ). This was done so that the results of the experiments could be compared. In the present research, the pulsing frequency ( $F$ ) of the square wave pulsating flow is found to be between 4 and 10 Hz, and  $Wo$  that corresponds to this frequency range is predicted to be between 30 and 48. For the purpose of this comparison, the average flow rate of CCT during the pulsating flow condition is the same as that during the steady flow state. The pulsating flow velocity profiles were all square waves. Moreover, the solenoid valve was manipulated to get the desired velocity profile. Figure 3 shows how the inlet velocity changes over time for a 4 Hz frequency as an example. According to Li et al. [23, 24], the changing inlet velocity is either the mean velocity plus the amplitude (the maximum velocity) or the mean velocity minus the amplitude (the minimum velocity), as shown in Fig. 3.

Here,  $U_{max}$  and  $U_{min}$  are the maximum and minimum velocities in the conical tube in a pulsating condition. To begin, the experimental apparatus and procedures were validated by comparing  $Nu$  for pulsating flow through the CCT to  $Nu$  published in the literature. According to the literature research, there is a lack of correlations needed to estimate

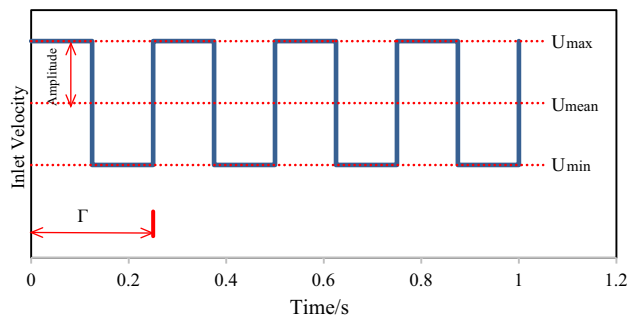


Fig. 3 The pulsation inlet velocity pattern [23, 24]

the Nu for pulsating flow in CCTs. The Nu for steady flow in CCTs, on the other hand, has a number of correlations in the literature. The current experimental data for steady flow in CCTs were validated using data from Abdelmagied [4] and Ali et al. [39].

The results of the comparison of experimental values of Nu with the correlated values of Nu are shown in Fig. 4. This figure shows how the experimental results for heat transfer and friction factor calculations agree well with earlier research.

## Heat transfer results

A group of experiments were carried out on CCTs in which the mass flow rate ranged from 0.03 to 0.09 kg s<sup>-1</sup>, the fluid temperature at the coil inlet was kept at 25 °C, and the pulsation frequency ranged from 4 to 10 Hz. The corresponding dimensionless parameters are  $0.02 \leq \lambda \leq 0.052$ ,  $1148 \leq De \leq 2983$  and  $30 \leq Wo \leq 48$ . Experiments were conducted with Re ranging from 4836 to 12,562. The critical Re for coiled tubes is displayed in Tables 4 and 5 of Appendix B, which are based on several published correlations. The relationship between the average Nu and the Dean number is seen in Fig. 5. It is clear from looking at Fig. 5 that the Nu values that are obtained under conditions of pulsating flow are higher than those that are obtained under conditions of steady flow ( $Wo = 0$ ) when the same value of De is used. This demonstrates that the square wave pulsating flow may further enhance the performance of the CCT with regard to heat transfer; nevertheless, it will also raise the flow resistance. It is important to keep in mind that in the pulsating condition, the influence that Wo has on Nu is more substantial when the De is large.

When the Wo was increased from 30 to 48 Hz while maintaining the same De, the increase in Nu was 36% for a CCT with  $\lambda = 0.02$ . Furthermore, the increase in Nu was

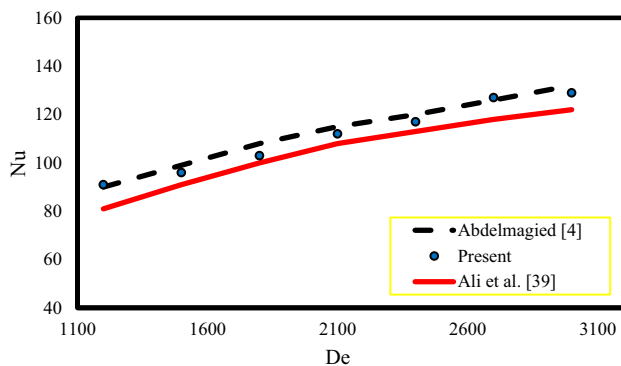


**Fig. 4** Validation of the experimental data for steady flow in CCT ( $\lambda = 0.036$ )

32% for  $\lambda = 0.036$  and 26% for  $\lambda = 0.052$ . This is mostly due to the fact that the action of secondary flow is primarily responsible for the enhancement in heat transfer that conical tubes provide [1–4]. The findings of previous studies [23, 40, 41] indicate that the secondary flow is responsible for a main role in the improvement of heat transfer even when the De is low.

Within the scope of this investigation, the condition of  $Wo = 30$  ( $F = 4$  Hz) represents the best possible outcome. When  $F$  is more than 4 Hz, there is a gradual drop in the average Nu value. This is due to the fact that the enhancement and expansion of secondary flow not only contribute to the enhancement of heat transfer but also increase flow resistance under situations that include pulsating flow. The construction of the vortex, its growth, and its expansion can only be achieved with the greatest possible balance by using the pulsating frequency that is ideal. This is necessary to ensure that the fluid is well mixed and to maximize

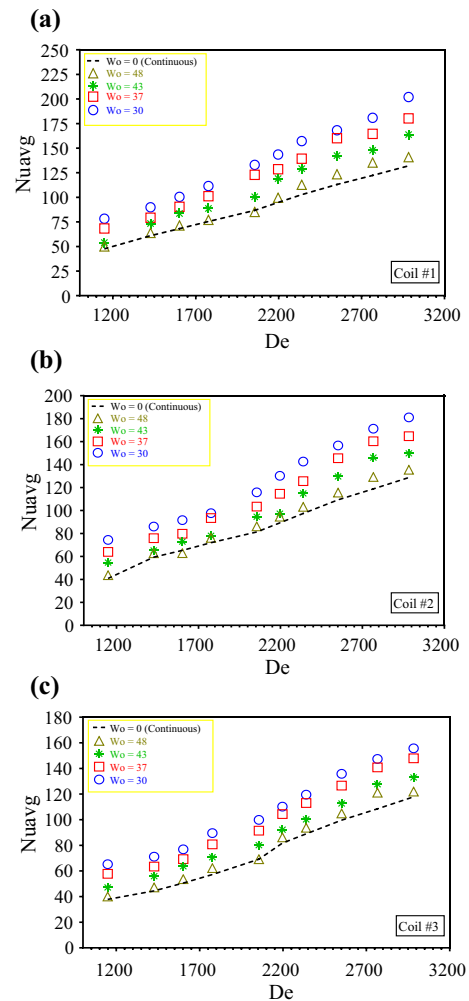


**Fig. 5** Variation of average Nusselt number with Dean number for  $\lambda = 0.02$ , **b**  $\lambda = 0.036$  and **c**  $\lambda = 0.052$



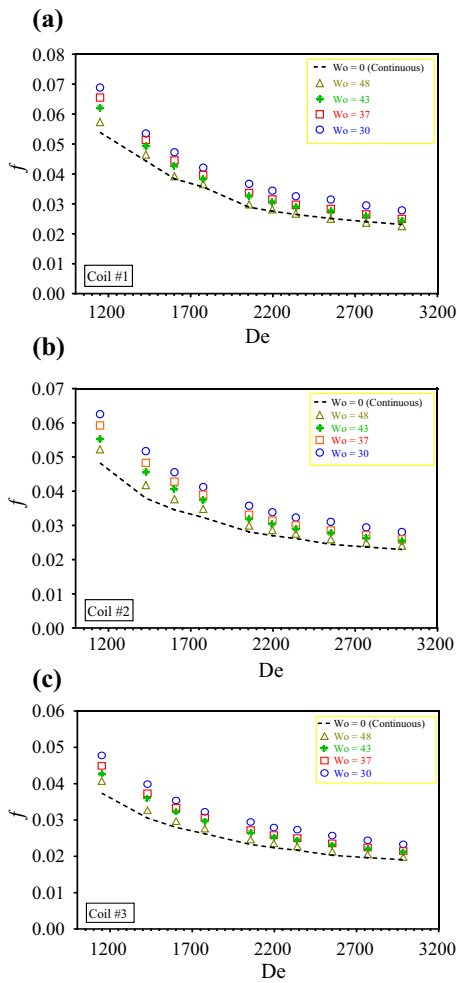


**Fig. 6** Variation of friction factor with Dean number for **a**  $\lambda=0.02$ , **b**  $\lambda=0.036$  and **c**  $\lambda=0.052$

the rate at which heat may be transferred [25]. As shown in Fig. 11 of Appendix A, every data point's error bar indicates the experimental uncertainty of the average Nu.

**Pressure drop results**

Two high-precision pressure sensors were attached to an Arduino circuit in order to detect the pressure drop through the conically coiled tubes at a variety of mass flow rates. The values of the friction coefficient are presented in Fig. 6 for a variety of pulsating flows ranging from 4 to 10 Hz, as well as for constant flow. Experiments were performed on CCTs in which the mass flow rate varied between 0.03 and 0.09 kg s<sup>-1</sup> and the fluid temperature at the coil inlet was maintained at 25 °C throughout all of the tests. The dimensionless

parameters that correspond to these ranges are as follows:  $0.02 \leq \lambda \leq 0.052$ ,  $1148 \leq De \leq 2983$  and  $30 \leq Wo \leq 48$ .

Figure 6 depicts the relationship between the average  $f$  and  $De$ . Figure 6 demonstrates that the friction factor values with the pulsating flow are better than those under steady flow ( $Wo=0$ ) while maintaining the same  $De$ , and this demonstrates that the square wave pulsating flow increases the heat transfer performance of the conical tube. Within the limits of this study, the  $Wo=30$  ( $F=4$  Hz) condition reflects the best result. The friction factor tends to decrease as the  $De$  increases. When the  $Wo$  was increased from 30 to 48 Hz, the rise in  $f$  for a CCT with  $\lambda=0.02$  was 22% at the same  $De$ . The increase of  $Nu$  was 23% when  $\lambda=0.036$ , and it was about 22%  $\lambda=0.052$ , this is due to an increase in centrifugal force and the consequent formation of vortices as a result of decreasing the torsion or rotational effect [41]. As shown in Fig. 12 of Appendix A, every data point's error bar indicates the experimental uncertainty of the friction factor.

**Correlation for average Nusselt number and friction factor**

Correlations were developed using the current experimental data to predict the average  $Nu$  and the Fanning friction factor inside the CCT. Using the least squares method, a correlation for the average Nusselt number was presented on the basis of experimental data. The correlation estimates the steady-state Nusselt number when the Womersley number tends toward infinite, as also confirmed by Khosravi-Bizhaem [17]. The average Nusselt number is correlated as a function of Womersley, Dean, and Prandtl numbers and coil torsion.

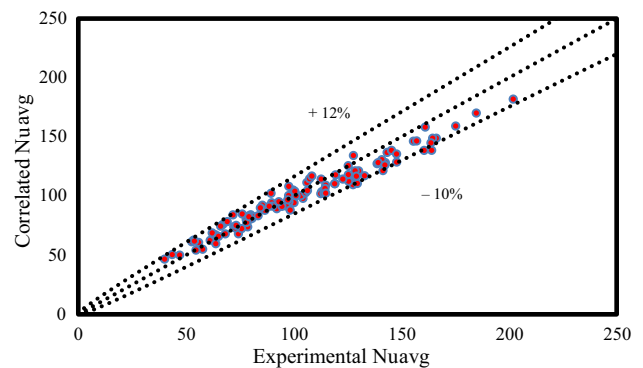


**Fig. 7** Comparison of experimental values for average  $Nu$  with that correlated by Eq. (15)

$$Nu_{avg} = (0.43 - 0.82Wo^{-0.6277})De^{0.658} \lambda^{-0.2344} Pr^{0.012} \quad (15)$$

Equation (15) is applicable for  $0.02 \leq \lambda \leq 0.052$ ,  $5.5 \leq Pr \leq 6$ ,  $1148 \leq De \leq 2983$  and  $30 \leq Wo \leq 48$ .

Figure 7 compares the experimental Nu to the correlated Nu, and it is obvious that the suggested correlations are in excellent agreement with the current experimental data, with a maximum deviation of 12%.

The friction factor is correlated as a function of Womersley, Dean numbers and coil torsion.

$$f = 42.97Wo^{-0.3616}De^{-0.8705} \lambda^{-0.2218} \quad (16)$$

Equation (16) is applicable for  $0.02 \leq \lambda \leq 0.052$ ,  $1148 \leq De \leq 2983$  and  $30 \leq Wo \leq 48$ .

Figure 8 compares the experimental  $f$  to the correlated  $f$ , and it is obvious that the suggested correlations are in excellent agreement with the current experimental data, with a maximum deviation of 15%.

### Performance evaluation criteria (PEC)

Performance evaluation criterion (PEC) of pulsating flow is the ratio of the Nusselt number ratio to the friction factor ratio at the same Dean number, as defined by Eq. (17). This ratio is used to assess the complete heat transfer improvement performance of square wave pulsating flow in a CCT.

$$PEC = \frac{\left(\frac{Nu_p}{Nu_s}\right)}{\left(\frac{f_p}{f_s}\right)^{\frac{1}{3}}} \quad (17)$$

where  $Nu_p$  and  $f_p$  represent the pulsating state's values.  $Nu_s$  and  $f_s$  represent the steady-flow state values. Figure 9 illustrates the experimental outcomes of the PEC of pulsating flow versus Womersley number for different coil torsion

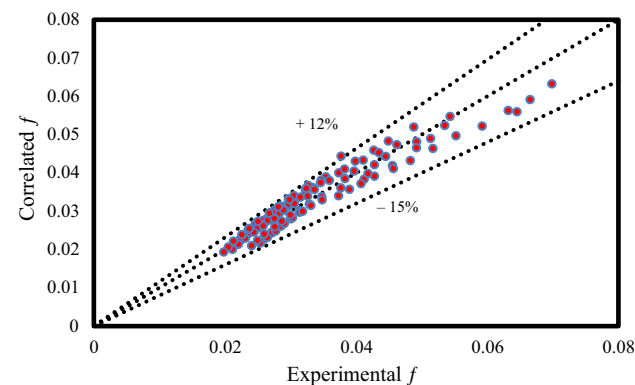


Fig. 8 Comparison of experimental values for friction factor with that correlated by Eq. (16)

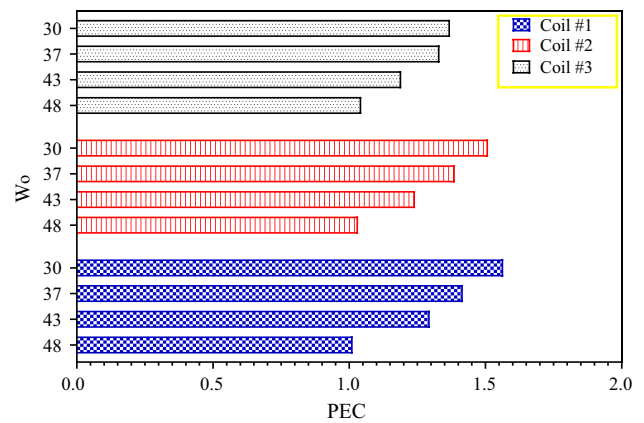


Fig. 9 The variations of PEC with Womersley number at different coil torsions

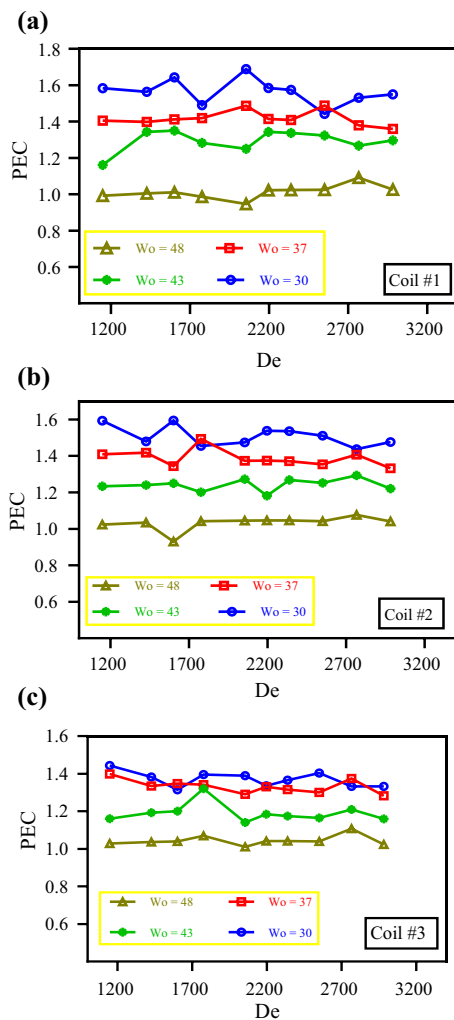


Fig. 10 Variation of PEC with Dean number for a  $\lambda=0.02$ , b  $\lambda=0.036$  and c  $\lambda=0.052$

values. As shown in Fig. 9, PEC improves by lowering the  $Wo$ . This is due to the fact that when there is pulsating flow, both the flow resistance and heat transfer increase, as the secondary flow becomes increasingly powerful. The PEC increased by 37% when the Womersley number was decreased from 48 to 30 for a CCT of  $\lambda=0.02$  (coil #1) with the same  $De$  value. For  $\lambda=0.036$  (coil #2), the PEC increased by 35%. Additionally, for  $\lambda=0.052$  (coil #3), the PEC increased by 28%.

Figure 10 depicts the relationship between performance evaluation criteria (PEC) and Dean number for a variety of pulsating frequencies. It is clear that the PEC values in the analysed scope are all bigger than unity, demonstrating the importance of using square wave pulsating flow to improve fluid heat transfer in conical tubes. Furthermore, it can be seen that in the range under study, the situation of  $Wo = 30$  is ideal. When  $Wo$  exceeds 30, the PEC value steadily decreases.

### Conclusions

The effects of pulsating flow on heat transfer and pressure drop in conical coiled tubes (CCTs) are the focus of this research. Three CCTs with various coil torsions ( $0.02 \leq \lambda \leq 0.052$ ) but the same curvature ratio ( $\delta = 0.0564$ ) were used in the experiments. The pulsating frequency ( $F$ ) of pulsating flow is between 4 and 10 Hz, and the corresponding Womersley number ( $Wo$ ) is estimated to be between 30 and 48 Hz. Moreover, the following conclusions might be drawn:

- Reducing the coil's torsion increases the heat transfer rate under similar operating conditions, whether the flow is constant or pulsating. This is because heat transfer is more efficient when secondary flows begin rapidly.
- The results demonstrate that the CCT-friction factor increases as the coil torsion decreases.
- The average Nusselt number increases as Dean number increases, although the friction factor typically decreases.
- The findings show that decreasing the pulsating frequency increases the heat transfer characteristics.
- A pulsating flow at 4 Hz ( $Wo=30$ ) was shown to promote heat transfer the most compared to all other frequencies investigated.
- The average  $Nu$  is increased by 23% at a frequency of 4 Hz ( $Wo=30$ ) and by decreasing coil torsion from 0.052 to 0.02 while the friction factor increased by 30%.

- Based on the Womersley, Dean, and Prandtl numbers and the coil torsion, the proposed correlations can accurately predict the average  $Nu$  and friction factor.
- Performance evaluation criteria (PEC) increased when the coil torsion decreased from 0.052 to 0.02.

### Appendices

#### Appendix A: Error bars

See Figs. 11 and 12.

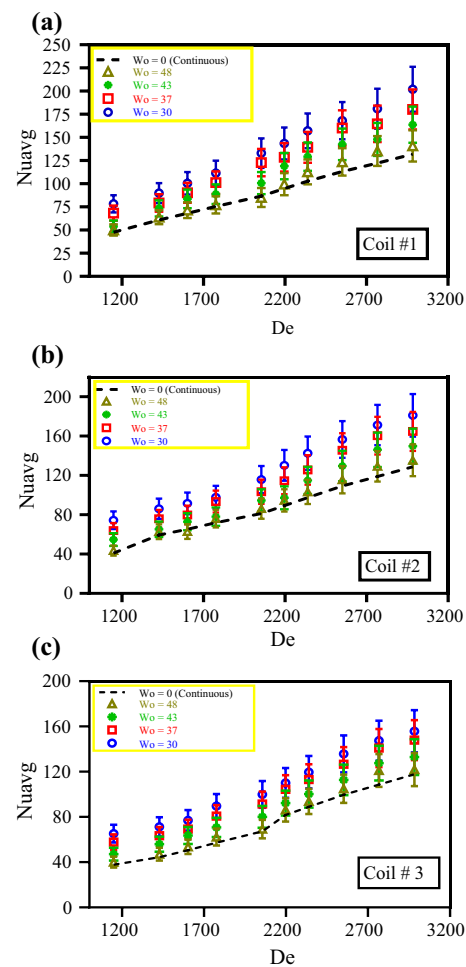
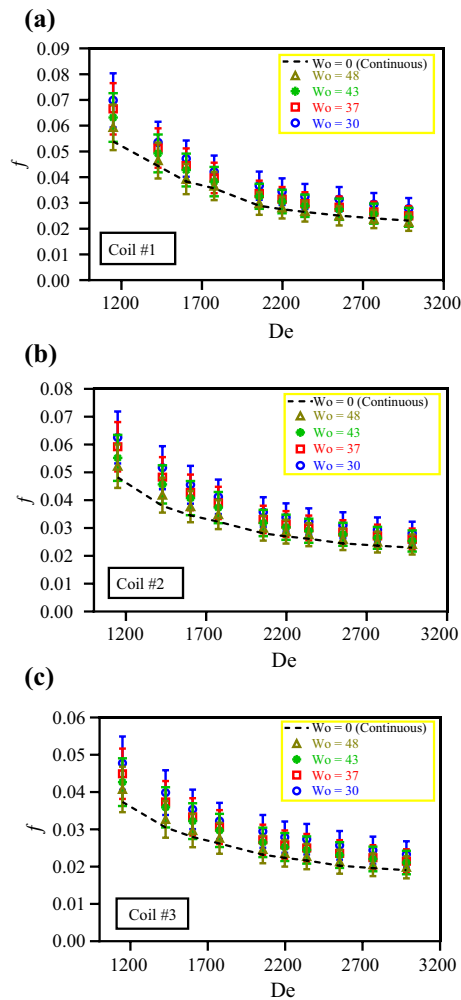


Fig. 11 Average  $Nu$  results with error bars for a  $\lambda=0.02$ , b  $\lambda=0.036$  and c  $\lambda=0.052$



**Fig. 12** Friction factor results with error bars for **a**  $\lambda=0.02$ , **b**  $\lambda=0.036$  and **c**  $\lambda=0.052$

## Appendix B: Critical Reynolds number

See Tables 4 and 5.

**Table 4** Critical Reynolds number correlations

Author	Operating conditions	Correlation
Schmidt [42]	$0.0123 \leq \delta \leq 0.2036$ $2000 \leq Re \leq 9000$	$Re_{cr} = 2300[1 + 8.6(\delta)^{0.45}]$
Ito [43]	$0.0005 \leq \delta \leq 0.1031$	$Re_{cr} = 2 \times 10^4 (\delta)^{0.32}$
Kubair and Varrier [44]	$0.0005 \leq \delta \leq 0.1031$ $2000 \leq Re \leq 9000$	$Re_{cr} = 1.273 \times 10^4 (\delta)^{0.2}$

**Table 5** Critical Reynolds number for coiled tubes

Coil no.	Coil curvature ( $\delta$ )	Coil torsion ( $\lambda$ )	$Re_{cr}$		
			Schmidt [42]	Ito [43]	Kubair and Varrier [44]
#1	0.0564	0.02	7723	7969	7162
#2		0.036			
#3		0.052			

**Funding** Open access funding provided by The Science, Technology & Innovation Funding Authority (STDF) in cooperation with The Egyptian Knowledge Bank (EKB).

**Open Access** This article is licensed under a Creative Commons Attribution 4.0 International License, which permits use, sharing, adaptation, distribution and reproduction in any medium or format, as long as you give appropriate credit to the original author(s) and the source, provide a link to the Creative Commons licence, and indicate if changes were made. The images or other third party material in this article are included in the article's Creative Commons licence, unless indicated otherwise in a credit line to the material. If material is not included in the article's Creative Commons licence and your intended use is not permitted by statutory regulation or exceeds the permitted use, you will need to obtain permission directly from the copyright holder. To view a copy of this licence, visit <http://creativecommons.org/licenses/by/4.0/>.

## References

1. Sheeba A, Akhil R, Prakash MJ. Heat transfer and flow characteristics of a conical coil heat exchanger. *Int J Refrig*. 2020;110:268–76. <https://doi.org/10.1016/j.ijrefrig.2019.10.006>.
2. Purandare PS, Lele MM, Gupta RK. Investigation on thermal analysis of conical coil heat exchanger. *Int J Heat Mass Transf*. 2015;90:1188–96. <https://doi.org/10.1016/j.ijheatmasstransfer.2015.07.044>.
3. Heyhat MM, Jafarad A, Changizi P, Asgari H, Valizade M. Experimental research on the performance of nanofluid flow through conically coiled tubes. *Powder Technol*. 2020;370:268–77. <https://doi.org/10.1016/j.powtec.2020.05.058>.
4. Abdelmagied MM. Investigation of the triple conically tube thermal performance characteristics. *Int Commun Heat Mass Transf*. 2020;119:104981. <https://doi.org/10.1016/j.icheatmasstransfer.2020.104981>.
5. Abdelghany MT, Elshamy SM, Salem MR, Abdellatif OE. Enhancement the Thermal performance of a Shell and Coil Heat exchanger with different Coil Geometries: Comparative experimental investigation. *Eng Res J*. 2020;1:57–65.
6. Elshamy SM, Abdelghany MT, Salem MR, Abdellatif OE. Energy and exergy analysis of shell and coil heat exchanger using water based  $Al_2O_3$  nanofluid including diverse coil geometries: an experimental study. *J Nanofluids*. 2020;9:13–23. <https://doi.org/10.1166/jon.2020.1727>.
7. Al-Salem K, Hosseini E, Nohesara A, Mehri M, Ali M, Almuzaiqr R, et al. Suggestion of new correlations for the exergy efficiency and coefficient of exergy performance of annulus section of conically coiled tube-in-tube heat exchangers. *Chem Eng Res Des*. 2019;152:309–19. <https://doi.org/10.1016/j.cherd.2019.10.002>.

8. Wang G, Wang D, Peng X, Han L, Xiang S, Ma F. Experimental and numerical study on heat transfer and flow characteristics in the shell side of helically coiled trilobal tube heat exchanger. *Appl Therm Eng.* 2019;149:772–87. <https://doi.org/10.1016/j.applthermaleng.2018.11.055>.
9. Abdelmagied M. Thermal performance characteristics of a triple spiral tube heat exchanger. *Chem Eng Process Process Intensif.* 2020;149:107707. <https://doi.org/10.1016/j.cep.2019.107707>.
10. Khosravi-Bizhaem H, Abbassi A, Salimpour MR, Zivari-Ravan A. Experimental study on heat transfer, entropy generation, and exergy destruction of Ag, MWCNT, and GO water-based nanofluids in helical tubes. *J Therm Anal Calorim.* 2022;147:2761–84. <https://doi.org/10.1007/s10973-021-10655-z>.
11. Mukesh Kumar PC, Chandrasekar M. Heat transfer and friction factor analysis of MWCNT nanofluids in double helically coiled tube heat exchanger. *J Therm Anal Calorim.* 2021;144:219–31. <https://doi.org/10.1007/s10973-020-09444-x>.
12. Heydari O, Miansari M, Arasteh H, Toghraie D. Optimizing the hydrothermal performance of helically corrugated coiled tube heat exchangers using Taguchi's empirical method: energy and exergy analysis. *J Therm Anal Calorim.* 2021;145:2741–52. <https://doi.org/10.1007/s10973-020-09808-3>.
13. Akgul D, Mercan H, Dalkilic AS. Parametric optimization of heat transfer characteristics for helical coils. *J Therm Anal Calorim.* 2022;147:12577–94. <https://doi.org/10.1007/s10973-022-11481-7>.
14. Basit Shafiq M, Allaudin U, Qaisrani MA, Rehman T, Ahmed N, Usman Mushtaq M, et al. Thermal performance enhancement of shell and helical coil heat exchanger using MWCNTs/water nanofluid. *J Therm Anal Calorim.* 2022;147:12111–26. <https://doi.org/10.1007/s10973-022-11405-5>.
15. Naphon P, Wiriyasart S, Arisariyawong T, Nakharintr L. ANN, numerical and experimental analysis on the jet impingement nanofluids flow and heat transfer characteristics in the micro-channel heat sink. *Int J Heat Mass Transf.* 2019;131:329–40. <https://doi.org/10.1016/j.ijheatmasstransfer.2018.11.073>.
16. Abdelghany MT, Elshamy SM, Sharafeldin MA, Abdellatif OE. Utilizing artificial neural networks to predict the thermal performance of conical tubes with pulsating flow. *Appl Therm Eng.* 2023. <https://doi.org/10.1016/j.applthermaleng.2023.120087>.
17. Khosravi-bizhaem H, Abbassi A, Ravan AZ. Heat transfer enhancement and pressure drop by pulsating flow through helically coiled tube: an experimental study. *Appl Therm Eng.* 2019;160:114012. <https://doi.org/10.1016/j.applthermaleng.2019.114012>.
18. Zohir AE, Abdel AA, Habib MA. Heat transfer characteristics and pressure drop of the concentric tube equipped with coiled wires for pulsating turbulent flow. *Exp Therm FLUID Sci.* 2015;65:41–51. <https://doi.org/10.1016/j.expthermfluidsci.2015.03.003>.
19. Pan C, Zhou Y, Wang J. CFD study of heat transfer for oscillating flow in helically coiled tube heat-exchanger. *Comput Chem Eng.* 2014;69:59–65. <https://doi.org/10.1016/j.compchemeng.2014.07.001>.
20. Pan C, Zhang T, Wang J, Zhou Y. CFD study of heat transfer and pressure drop for oscillating flow in helical rectangular channel heat exchanger. *Int J Therm Sci.* 2018;129:106–14. <https://doi.org/10.1016/j.ijthermalsci.2018.02.035>.
21. Zhang H, Li S, Cheng J, Zheng Z, Li X, Li F. Numerical study on the pulsating effect on heat transfer performance of pseudo-plastic fluid flow in a manifold microchannel heat sink. *Appl Therm Eng.* 2018;129:1092–105. <https://doi.org/10.1016/j.applthermaleng.2017.10.124>.
22. Wei JY, Zheng LX. Effect on the flow and heat transfer characteristics for sinusoidal pulsating laminar flow in a heated square cylinder. 2014;849–64. <https://doi.org/10.1007/s00231-014-1294-4>
23. Li Y, Yu Q, Yu S, Zhang P, Zhang J. Numerical investigation and mechanism analysis of heat transfer enhancement in a helical tube by square wave pulsating flow. *Heat Mass Transf und Stoffuebertragung.* 2023;59:21–37.
24. Li Y, Yu Q, Yu S, Gong B, Zhang J. Numerical investigation of pulsating flow structures and heat transfer enhancement performance in spherical corrugated helical tube. *Appl Therm Eng.* 2022;213:118647. <https://doi.org/10.1016/j.applthermaleng.2022.118647>.
25. Guo W, Li G, Zheng Y, Dong C. The effect of flow pulsation on Al<sub>2</sub>O<sub>3</sub> nanofluids heat transfer behavior in a helical coil: a numerical analysis. *Chem Eng Res Des.* 2020;156:76–85. <https://doi.org/10.1016/j.cherd.2020.01.016>.
26. Naphon P, Wiriyasart S. Pulsating TiO<sub>2</sub>/water nanofluids flow and heat transfer in the spirally coiled tubes with different magnetic field directions. *Int J Heat Mass Transf.* 2017;115:537–43. <https://doi.org/10.1016/j.ijheatmasstransfer.2017.07.080>.
27. Naphon P, Arisariyawong T, Wiriyasart S, Srichat A. ANFIS for analysis friction factor and Nusselt number of pulsating nanofluids flow in the fluted tube under magnetic field. *Case Stud Therm Eng.* 2020;18:100605. <https://doi.org/10.1016/j.csite.2020.100605>.
28. Naphon P, Wiriyasart S. Pulsating flow and magnetic field effects on the convective heat transfer of TiO<sub>2</sub>-water nanofluids in helically corrugated tube. *Int J Heat Mass Transf.* 2018;125:1054–60. <https://doi.org/10.1016/j.ijheatmasstransfer.2018.05.015>.
29. Naphon P, Wiriyasart S. Experimental study on laminar pulsating flow and heat transfer of nanofluids in micro-fins tube with magnetic fields. *Int J Heat Mass Transf.* 2018;118:297–303. <https://doi.org/10.1016/j.ijheatmasstransfer.2017.10.131>.
30. Naphon P, Wiriyasart S, Arisariyawong T. Artificial neural network analysis the pulsating Nusselt number and friction factor of TiO<sub>2</sub>/water nanofluids in the spirally coiled tube with magnetic field. *Int J Heat Mass Transf.* 2018;118:1152–9. <https://doi.org/10.1016/j.ijheatmasstransfer.2017.11.091>.
31. Shiravi AH, Shafiee M, Firoozzadeh M, Bostani H, Bozorgmehrian M. Experimental study on convective heat transfer and entropy generation of carbon black nanofluid turbulent flow in a helical coiled heat exchanger. *J Therm Anal Calorim.* 2021;145:597–607. <https://doi.org/10.1007/s10973-020-09729-1>.
32. Khanlari A, Adnan S, Ibrahim H. Upgrading the performance of shell and helically coiled heat exchangers with new flow path by using TiO<sub>2</sub>/water and CuO–TiO<sub>2</sub>/water nanofluids. *Int J Therm Sci.* 2023. <https://doi.org/10.1016/j.ijthermalsci.2022.107831>.
33. Sundar LS, Shaik F. Heat transfer and exergy efficiency analysis of 60% water and 40% ethylene glycol mixture diamond nanofluids flow through a shell and helical coil heat exchanger. *Int J Therm Sci.* 2023;184:107901. <https://doi.org/10.1016/j.ijthermalsci.2022.107901>.
34. Cengel YA. Heat Transference a Practical Approach MacGraw-Hill. 2004;4:874. [https://doi.org/10.1007/978-3-642-20279-7\\_5](https://doi.org/10.1007/978-3-642-20279-7_5).
35. Gilli M, Maringer D, Schumann E. Numerical methods and optimization in finance. *Numer Methods Optim Financ.* 2019;1–614.
36. Bejan A. Convection heat transfer. Hoboken: Wiley; 2013.
37. Barker G. Chapter 18 - Pipe sizing and pressure drop calculations. In: Barker G, editor. *Eng Guid to Plant Layout Pip Des Oil Gas Ind.* Gulf Professional Publishing; 2018. p. 411–72. <https://doi.org/10.1016/B978-0-12-814653-8.00018-7>.
38. Holman JP, Burr Ridge B, Dubuque I, Madison I, New York. *Experimental methods for engineers.* 2012.
39. Ali M, Rad MM, Nuhait A, Almuzaiqer R, Alimoradi A, Tlili I. New equations for Nusselt number and friction factor of the annulus side of the conically coiled tubes in tube heat exchangers. *Appl Therm Eng.* 2020;164:114545. <https://doi.org/10.1016/j.applthermaleng.2019.114545>.

40. Li YX, Wang X, Zhang J, Zhang L, Wu JH. Comparison and analysis of the arrangement of delta winglet pair vortex generators in a half coiled jacket for heat transfer enhancement. *Int J Heat Mass Transf.* 2019;129:287–98. <https://doi.org/10.1016/j.ijheatmasstransfer.2018.09.109>.
41. Salem MR, Elshazly KM, Sakr RY, Ali RK. Effect of coil torsion on heat transfer and pressure drop characteristics of shell and coil heat exchanger. *J Therm Sci Eng Appl.* 2016;8:1–7. <https://doi.org/10.1115/1.4030732>.
42. Schmidt EF. Wärmeübergang und Druckverlust in Rohrschlangen. *Chemie Ing Tech.* 1967;39:781–9. <https://doi.org/10.1002/cite.330391302>.
43. Ito H. Pressure losses in smooth pipe bends. *J Basic Eng.* 1959;123–134.
44. Kubair V, Varrier CBS. Pressure drop for liquid flow in helical coils. *Trans Indian Inst Chem Eng.* 1961;14:93–7.

**Publisher's Note** Springer Nature remains neutral with regard to jurisdictional claims in published maps and institutional affiliations.